Microsystem Technologies (2020) 26:2487–2498
https://doi.org/10.1007/s00542-020-04789-7

TECHNICAL PAPER

A powerless iron oxide based magnetometer

Tyler Coughlin[1] · Reza Rashidi[1]

Received: 7 February 2020 / Accepted: 18 February 2020 / Published online: 22 February 2020

Abstract
This paper demonstrates a novel device visualizing and determining magnetic fields in six different directions. The device can be used in applications such as remote real estate construction sites requiring an inexpensive and powerless method of detection and determination of a magnetic field. The magnetometer uses magnetic properties of nanostructured iron oxide to aid in visualizing the location, direction and strength of magnetic fields. The device utilizes various sizes of permanent magnets which attract and hold the iron oxide nanoparticles in mini channels when there is no external magnetic field in the environment. Upon exposing to a magnetic field stronger than the magnetic strength of the holding magnet, the particles are repelled toward the external field. The magnetometer was fabricated by making tubes in an acrylic block in three dimensions and six directions, and filling them with iron oxide nanoparticles. The inner ends of the tubes were plugged by various sizes of permanent magnets and the outer ends were sealed by glass sheets. The device was exposed to different external fields created by various permanent magnets and successfully tested using a reference Gauss meter. The device was capable of identifying external magnetic fields up to 1455 Gauss.

1 Introduction

Magnetometers are used to measure the direction and strength of magnetic fields. The ability to measure magnetic fields can be used in several fields of science from biology to physics, such as applications that include archaeology, health care monitoring, and aerospace (Budker 2003). Most of the current magnetometers directly detect the magnetic flux density of a medium and display it in Gauss or Tesla units (Schwindt et al. 2004; Auster et al. 2008). Magnetic fields are transparent, and in order to be seen, magnetic materials such as iron particles and ferrofluid are required to be brought close to the field where the particles move and form the direction of the field. Magnetometers can be very precise in measuring low frequency magnetic fields and strengths (Cai et al. 2012). In general, there are two types of magnetometers, scalar and vector magnetometers. Scalar Magnetometers include proton precession magnetometers (Liu et al. 2017), overhauser effect magnetometers (Li et al. 2016) and ionized gas magnetometers (Cochrane et al. 2016). They use a scalar value of magnetic flux to determine the field strength while vector magnetometers measure both direction and magnitude of a magnetic field (Leger et al. 2009). Vector based magnetometers include fluxgate magnetometers (Pang et al. 2013), SQUID (Superconducting Quantum Interference Device) magnetometers (Budker and Romalis 2007), search-coil magnetometers (Le Contel et al. 2016), rotating coil magnetometers (Russenschuck 2017) and magneto resistive magnetometers (Brown et al. 2012). Examples of devices that exploit magnetic fields include precision magnetic field sensors (Zu et al. 2012), electric current sensors (Xu et al. 2011), position tracker sensors (Roetenberg et al. 2007), pressure sensors (Meyners et al. 2009), torque sensors (Kohout et al. 2007) and force sensors (Cui et al. 2012).

Magnetic nanoparticles such as iron oxide have been studied for decades and used into a growing number of applications that utilize them for their magnetic properties (Teja and Koh 2009). These particles are utilized in several applications and devices associated with molecular and cellular imaging (Bulte and Kraitchman 2004; Qiang et al. 2006), catalysts (Li et al. 2008; Cabrera et al. 2008; Hermanek et al. 2007; Uddin et al. 2008), biomedicine (Tartaj et al. 2011; Wang 2011) and sensors (Liu et al. 2010; Biswal 2011; Kaushik et al. 2009). These iron oxide particles can also be used in actuators such that when a

✉ Reza Rashidi
rashidr@alfredstate.edu

[1] Department of Mechanical and Electrical Engineering Technology, State University of New York, Alfred State College, Alfred, NY 14802, USA

magnetic field is present, the particles can be forced, moving objects. In addition, some magnetometers utilize magnetic fluids or elements; for example, ferrofluid based magnetometers use a tube filled with the fluid. When exposed to a magnetic field, the ferrofluid reacts to the field which is displayed as the field strength (Jian et al. 2006). Some existing magnetic fluid-based magnetometers use a quartz resonator filled with ferrofluid, which vibrates when they are brought to a magnetic field. These magnetometers measure the frequency shift of the resonator as a function of the applied magnetic field (Hatipoglu and Tadigadapa 2015). Other magnetometers utilize a ferrofluid simultaneously subjected to two orthogonal magnetic fields, an exciting field and an external field whose strength is determined. The ferrofluid generates an induced electromotive force which is detected by a pick-up coil around the ferrofluid. These magnetometers operate at frequencies below 10 kHz (Baltag 2013). Some other types of magnetometers utilize infrared wavelength spectrometers to measure magnetic flux density (Homa and Pickrell 2014). SQUID magnetometers have also been utilized with magnetic fluid for magnetic sensing (Weinstock 2012; Lee et al. 1991). They have been used to study human brain and electrical impulses associated with dental pain, auditory, and visually evoked brain activity (Ilmoniemi et al. 1984). In addition, they are utilized to aid bio-magnetic image sensing by constructing a magnetometer array (Fujimaki et al. 1988; Kominis et al. 2003). Another design employs photonic crystal fibers filled with ferrofluid that refracts within the fibers when an external magnetic field is present. The field is detected by the transmission light intensity through the device (Gao et al. 2013). A similar magnetometer that also uses light has a V-shaped groove that is filled with magnetic fluids. Light is propagated through the groove and the position of the light determines the strength of the applied magnetic field (Ji et al. 2012). Other devices utilizing ferrofluid have fiber Bragg gratings (FBG) which are very sensitive to the refractive index of magnetic fluid and are affected by an external magnetic field (Zhou et al. 2011; Dai et al. 2011; Gao et al. 2010). Furthermore, diamonds have been used in magnetometers to detect weak magnetic fields by manipulating the nitrogen-vacancy centers within the structure of the diamond (Taylor et al. 2008). These devices all aid in determining the field strength. The drawback of these devices is that their fabrication require several steps and may need a large array of equipment and devices. In addition, the devices usually require a power supply to operate. These make the devices expensive to be used in applications that require low cost devices. It would be beneficial for one to be able to visually check the existence of a field in real time and measure the strength and direction of the field using a device that requires no power, particularly in remote areas.

This paper presents a novel concept of a powerless magnetometer that is used to detect and characterize magnetic fields. Various sensor developments have been demonstrated by this group (Duell et al. 2018; Rashidi et al. 2019; Bower et al. 2018). The design utilizes a minimum number of parts including permanent magnets, iron oxide nanoparticles and acrylic blocks, and could easily be fabricated. The device can be used in several applications that require the ability to measure magnetic field magnitude and direction. As an example, the device can be employed in the construction industry to identify potential harmful magnetic fields near buildings being constructed. Furthermore, they could be used to detect magnetic fields inside buildings. They are maneuverable to aid in detecting where a field is located and potentially determine the range of a magnetic field. The device can also be used within a hospital setting where MRI (magnetic resonance imaging) devices create powerful magnetic fields to image detailed pictures of internal body structures. The magnetometer could be utilized to detect if a magnetic field leaves the room where the tests are being completed. This could aid in having proper signage in areas where a magnet could manipulate a device implanted in a body, such a Pacemaker or Implantable Cardioverter Defibrillator. The powerless magnetometer can also be used as a teaching tool to aid in demonstrating 3D magnetic fields. With a scaled down version of the device, there is the potential to detect magnetic fields in an environment. A device in this respect would be inexpensive and easily be able to detect a range of the needed clearance.

2 Design

The visual iron oxide magnetometer was designed using SolidWorks as shown in Fig. 1a. The design is capable of monitoring magnetic fields in three axes and six directions. The design consists of seven solid clear acrylic blocks, comprised of a larger core block and two outer blocks for each axis. The clear blocks help visualize the movement of magnetic particles. The two smaller blocks in each axis are used to monitor magnetic field in positive and negative direction of the axis. The smaller outer blocks are 46 mm × 46 mm × 13 mm with four cut through holes to act as reservoirs for the magnetic fluid as shown in Fig. 1b. The holes were cut through the block in a fashion to have 6-axis tubes for each size of permanent magnet. The holes have a 6.35 mm diameter. The larger core block which acts as a mechanical support is a 46 mm × 46 mm × 46 mm solid acrylic block. The permanent magnets used need to have a minimum 19 mm distance between them so that they do not interfere with each other. As a result, the reservoirs are spaced adequately to prevent interference.

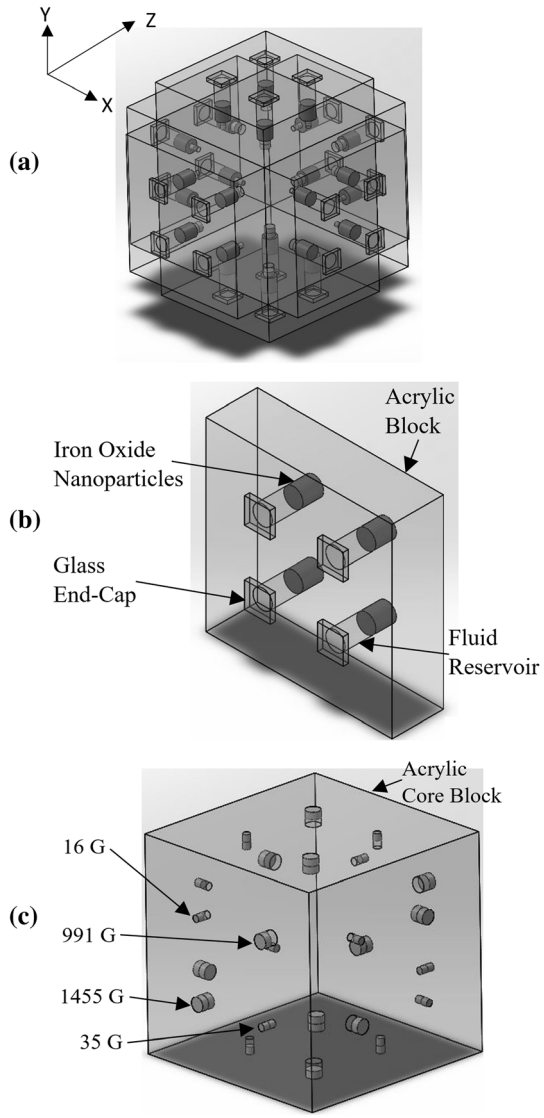

Fig. 1 SolidWorks assemblies of the visual iron oxide magnetometer (**a**), outer acrylic block assembly (**b**), core acrylic block assembly (**c**)

The four sizes of permanent magnets used were identified with pull strengths of 0.1 lbs, 0.2 lbs, 0.5 lbs and 1.0 lbs, producing magnetic fields of 16 G, 35 G, 991 G, and 1455 G, respectfully, as tested using a Gauss meter. The outer ends of the holes are capped with 12.7 mm × 12.7 mm pieces of glass using an acrylic epoxy. The inner ends of the holes in the blocks are sealed by the core solid acrylic block that acts as the main frame of the device. Four permanent magnets with different pull strengths are plugged into each faces of the core block where the holes end. Figure 1c shows the core block used to mount the six smaller blocks. The magnets used to hold the iron oxide are in-set within the block. Each side of the block has four magnet sets with the aforementioned pull strengths.

Figure 2 shows the working principle of the visual iron oxide magnetometer in a direction for a size of the

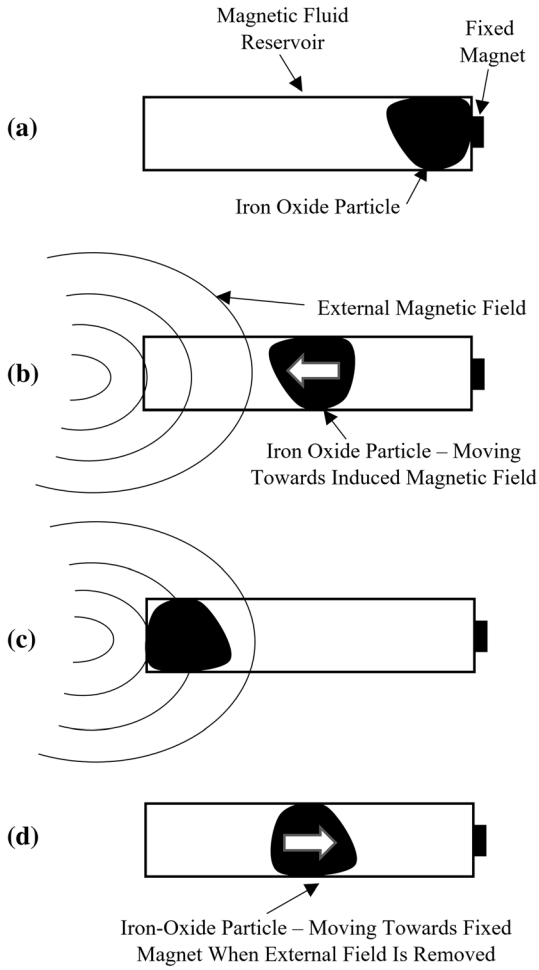

Fig. 2 Working principle of the visual iron oxide magnetometer

permanent magnet. First, in a lack of an external magnetic field, the permanent magnets attract and hold the iron oxide particles as shown in Fig. 2a. Upon presence of an external magnetic field stronger than the permanent magnet in the device, the iron oxide particles begin moving towards the field as shown in Fig. 2b. This magnetic field must be stronger than the permanent magnet that is attracting the particles at the end of the reservoir. The particles are completely attracted by the external field and accumulated at the outer end of the hole where the glass piece is sealed as shown in Fig. 2c. When the external magnetic field is removed, the permanent magnet attracts the iron oxide particles back towards the inner end of the hole as shown in Fig. 2d. This cycle can be repeated for the other three sizes of permanent magnets. When the external field is stronger than the smaller 16 G magnet, none of the particles in all four sets of the holes are separated from the permanent magnets. When the external field is between 16 and 35 G, only the iron oxide particles in the hole containing 16 G magnet will move towards the external field and the rest are still attached to the other three magnets. When a stronger

external field between 35 and 991 G is applied, iron oxide particles in both holes containing 16 G and 35 G will move towards the external field. A similar process can be described for other situations. All six blocks containing similar four sizes of magnets can act in a similar fashion. As a result, one can determine the direction and the range of an external magnetic field using the device.

3 Fabrication

The iron oxide-based powerless magnetometer was fabricated using clear acrylic blocks. The core block has four bored out holes on each face. These holes are drilled deep enough to have the magnets sit flush with the face of the block. The magnets used have a diameter of 1.6 mm (corresponding to 16 G) and 3.2 mm (corresponding to 991 G) and both magnets are 1.6 mm thick. To achieve the pull strength of 0.2 lb (corresponding to 35 G), two similar 1.6 mm diameter magnets are stacked on each other. Similarly, to achieve the pull strength of 1.0 lb (corresponding to 1455 G), two similar 3.2 mm diameter magnets are stacked on each other. The magnets were bonded into their holes using a clear adhesive. The six smaller blocks on faces of the core block act as the reservoirs for the iron oxide nanoparticles. These reservoirs have a diameter of 12.7 mm. The holes were not drilled all the way through the block, therefore assembling the blocks together was easier and sealing the reservoirs could be more effectively accomplished. Once all the blocks were cut, they had to be sanded and polished with 80, 120, 180, 220, 400, 600 and 800 grit sand papers so that the clear attribute of the acrylic block could be achieved. The reservoirs are filled with of 58.9 mm^3 of synthetic black iron oxide (Fe_3O_4) and filled the rest of the way with tap water. The water acts as a medium to aid the iron oxide in moving from one side of the reservoir to the other and to avoid the iron oxide sticking to the walls of the reservoir. The end of each reservoir is capped with a sheet of glass bonded to the surface of the acrylic block. Once all the smaller acrylic blocks were fabricated, they were then bonded to the core block faces using a clear adhesive. Figure 3 shows a photo of the fabricated visual iron oxide-based powerless magnetometer. On the device there are four different colored stickers placed in the corners of each block. This is to indicate which fixed magnet is affixed under the reservoir next to it. The color code is as follows: Blue—16 G, Yellow—35 G, Pink—991 G, and Orange—1455 G.

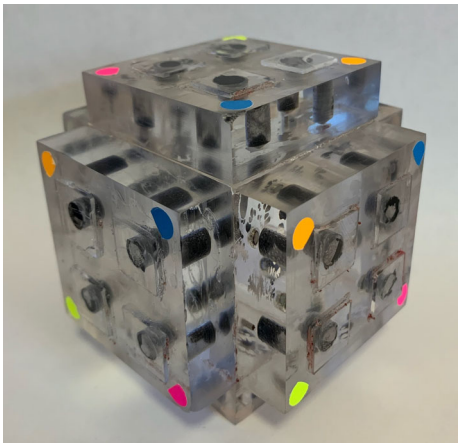

Fig. 3 Isometric view of fabricated visual iron-oxide magnetometer

4 Results and discussion

The powerless visual iron oxide magnetometer has fixed permanent magnets that attract and hold the iron oxide nanoparticles inside the reservoirs. This not only acts as a bias field to reset the nanoparticles position, but also act as a baseline magnetic field. The functionality of the fabricated magnetometer was first tested. When a strong permanent magnet with a 3839 G as an external magnetic field is gradually brought close to the device in Y axis face, the iron oxide particles pulls away from the device fixed magnets to the outer ends of the reservoirs, one at a time. Figure 4 shows the movement of nanoparticles within the reservoirs in the Y axis direction in five different steps, from before an external magnetic field was introduced to where all the iron oxide in the reservoirs were displaced. When the magnet is far away from the device face, the iron oxide nanoparticles in none of the reservoirs are pulled towards the external magnet as shown in Fig. 4a. As the magnet gets closer to the device face, the particles in the reservoir with the 16 G magnetic field first moves as shown in Fig. 4b. The closer the stronger magnetic field gets, the particles in the next reservoir with an increased magnetic field (35 G) than the first one is displaced off the fixed magnet as shown in Fig. 4c. Again, as the distance to the block shortened, the particles in the 991 G reservoir are moved (Fig. 4d) and finally the ones in the 1455 G reservoir are displaced (Fig. 4e). The order of nanoparticles movement in the reservoirs is labeled as 1–4 in Fig. 4. The orientation remained constant when testing. It is to be noted that when testing in the X or Z direction, gravity neither aids or hurts the ability for the external magnet to pull the iron oxide away from the device magnets. However, in the positive Y direction, it takes slightly more force to pull up the iron oxide particles due to gravity force added to the device magnet force, trying to keep the

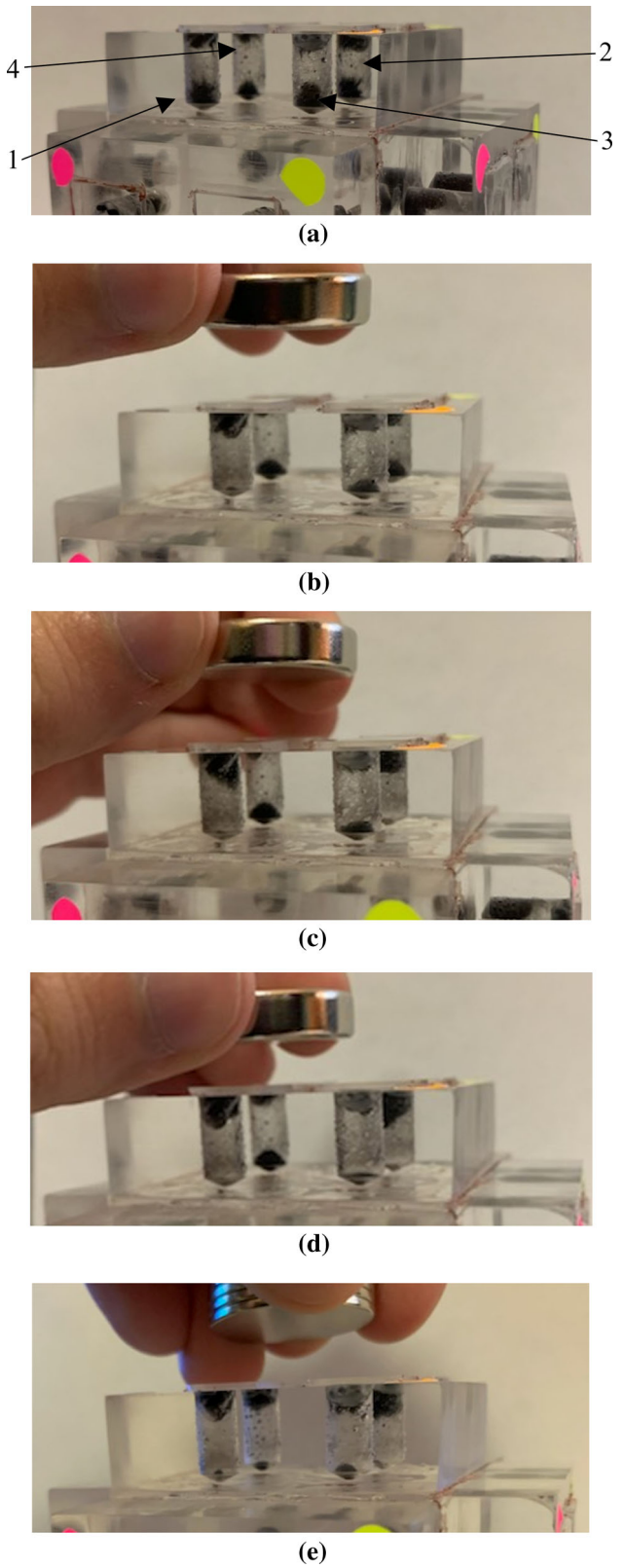

Fig. 4 Movement of the iron oxide nanoparticles in the reservoirs when presented to an external magnetic field. Numbers 1–4 show the order of reservoirs being actuated

particles in the bottom of the reservoir. In the negative Y direction, gravity is aiding the external magnet in pulling the iron oxide particles as gravity and external field forces are in the same direction.

To determine the critical distance between external and device magnets at which the external magnetic field will take over and begin pulling the iron oxide particles away from the device magnets, Gauss reading tests were performed at various distances from each device magnet along with four sets of larger permanent magnets as an external actuators using a Gauss meter (AlphaLab Inc.). The test results were used to characterize the magnetic field of the magnets and so the device. The magnets are called out by their maximum Gauss reading on their flat surfaces. The external magnets tested have different maximum Gauss readings of 3839 G, 3031 G, 2858 G and 2489 G. The four external magnets have a 25.5 mm diameter and thicknesses of 6.4 mm, 4.8 mm, 3.2 mm and 1.6 mm, respectfully.

The 2858 G magnetic field tested consists of three 1.6 mm thick magnets. Figure 5 compares the results of magnetic field readings as a function of distance from the magnet surface for all four external magnets to test the device. Due to the thickness of the outer acrylic blocks enclosing the fluid reservoirs, the smallest distance the external magnets can get to the fixed magnets is 12.7 mm. In order for the external magnet to start taking over and pull the iron oxide nanoparticles away from the fixed magnet, it must have a higher Gauss value than the fixed magnet does on its surface. This is because the particles rest on the face of the fixed magnet and has its maximum magnetic field value there.

Figure 6 shows the results of magnetic field readings as a function of distance from the magnet surface for all four types of the fixed magnets used within the device. Each external magnet was tested on the device against each of the fixed magnets. Shown in Figs. 7, 8, 9 and 10 are the magnetic field versus the distance from the surface of fixed magnets comparing the results of tests on each of the external magnets and all four fixed magnets. There will be a critical distance of the external magnet from any of the fixed magnets when the external magnet is moved towards the fixed magnet in the device. At this distance the magnetic field of the external magnet becomes greater than that of the fixed magnet at its surface where the nanoparticles are initially located (zero distance) and the external magnet would be able to overcome the force on the particles provided by the fixed magnet and move the particles.

As shown in Fig. 7, when the 2489 G external magnet is approximately 65 mm away from the 16 G fixed magnet, it applies a stronger field and begins moving the iron oxide nanoparticles towards itself. It is assumed that the initial distance of the external magnet from the fixed magnets is 80 mm as indicated in Fig. 7a. Similarly, when the external

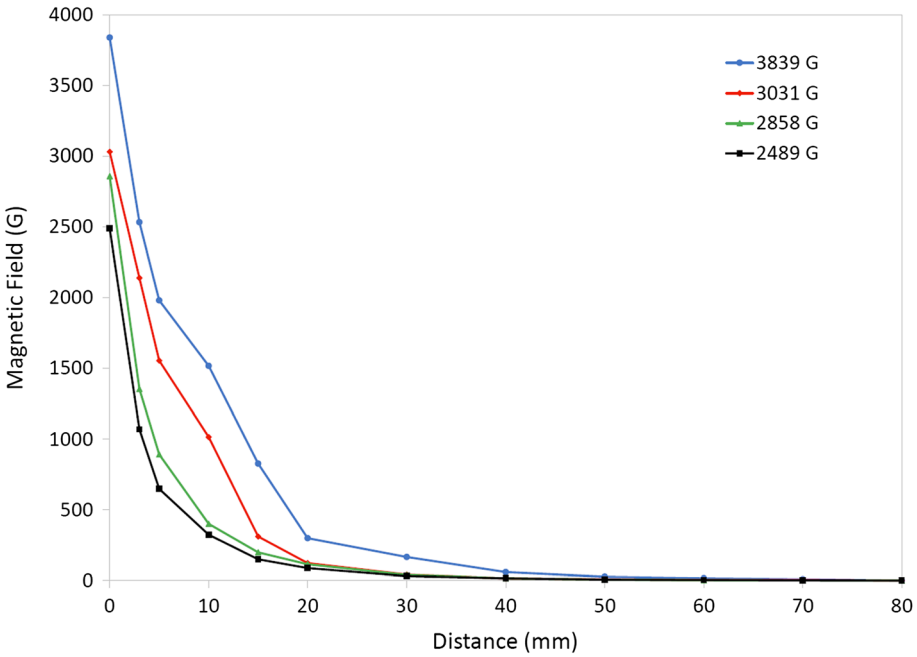

Fig. 5 External magnetic field readings over various distances

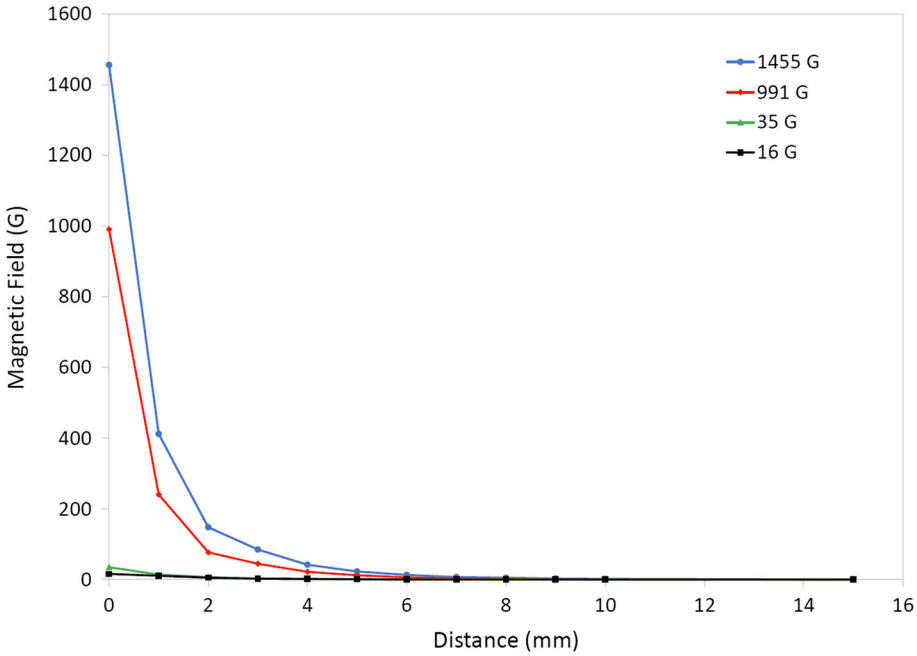

Fig. 6 Fixed magnetic field readings over various distances

magnet is approximately 59 mm away from the 35 G fixed magnet it takes over and pulls the nanoparticles. When tested against the 991 G and 1455 G fixed magnets on the device, the 2489 G external magnet does not move the nanoparticles because the magnets cannot get closer than 12.7 mm, the thickness of the outer acrylic block. The external magnets of 991 G and 1455 G would take over if they could get closer than 12 mm and 7 mm, respectively.

As shown in Fig. 8, when the 2858 G external magnet is roughly 65 mm away from the 16 G fixed magnet it creates a stronger magnetic field and pulls the iron oxide particles. It is assumed that the initial distance of the external magnet from the fixed magnets is 80 mm as indicated in Fig. 8a. When it is approximately 61 mm away from the 35 G fixed magnet it begins to move the particles towards itself in the reservoir. Furthermore, when it is roughly 18 mm away from the 991 G fixed magnet, it would take over. Again, the 2858 G external magnet cannot move the particles attached to 1455 G fixed magnet in the reservoir. The

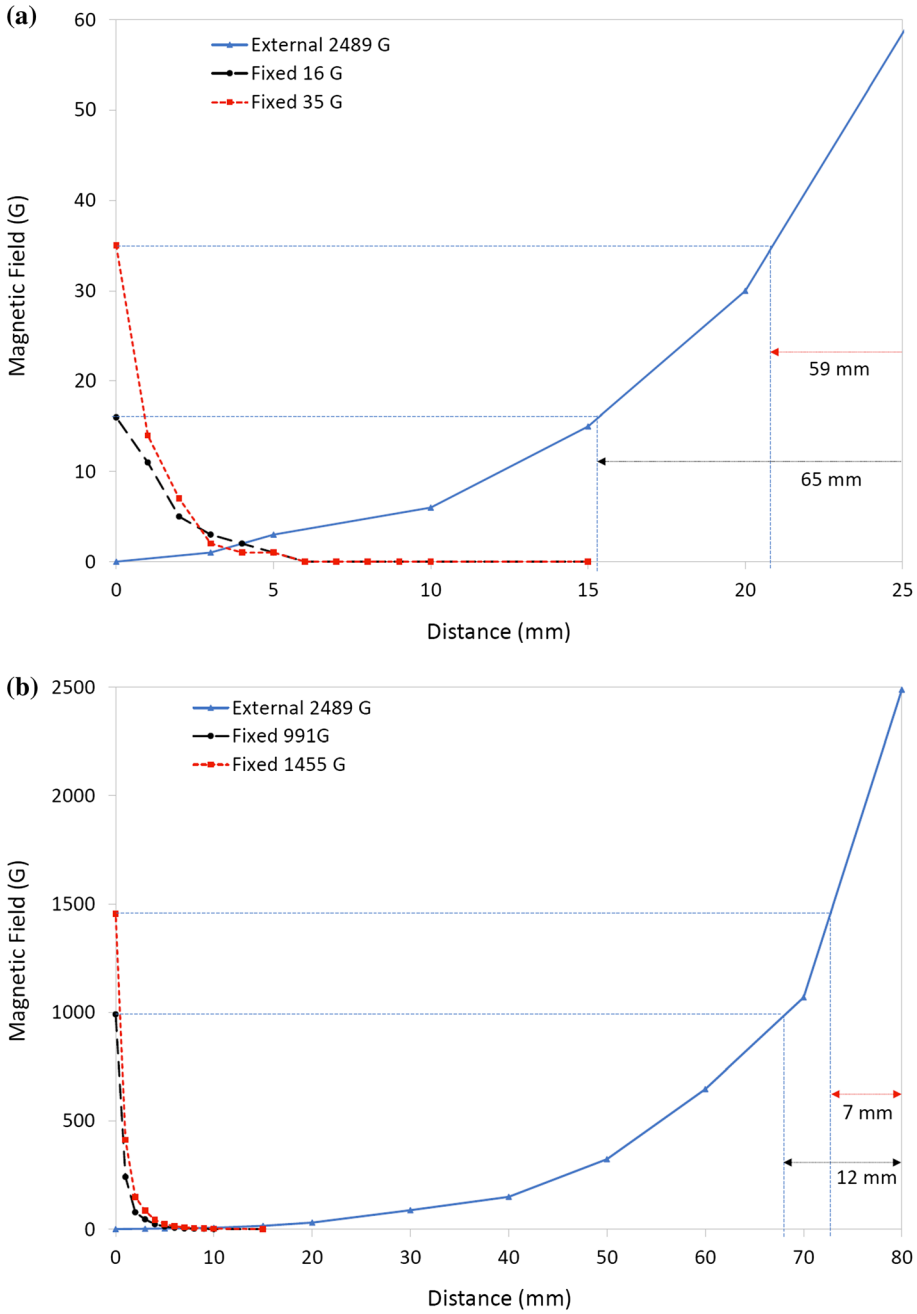

Fig. 7 A comparison between magnetic fields of the 2498 g external magnet and four fixed magnets. The external magnet is initially located at 80 mm away from the fixed magnets

minimum distance to take over the force is within the reservoir block (9 mm) and cannot be obtained.

As shown in Fig. 9, when the 3031 G external magnet is approximately 65 mm away from the 16 G fixed magnet, the nanoparticles begin to move away from the fixed magnet because the magnetic field of the external magnet becomes stronger. It is assumed that the initial distance of the external magnet from the fixed magnets is 80 mm as indicated in Fig. 9a. A similar process happens for the 35 G fixed magnet at relatively 62 mm away. The iron oxide nanoparticles attached to the 991 G fixed magnet moves towards the 3031 G external magnet at a 30 mm distance. As for the strongest fixed magnet, 1455 G, it would allow the iron oxide particles move away when it has a distance of 22 mm.

As shown in Fig. 10, when the 3839 G external magnet is brought within 75 mm of the 16 G fixed magnet surface, the nanoparticles begin to move. It is assumed that the initial distance of the external magnet from the fixed magnets is 80 mm as indicated in Fig. 10a. When it is

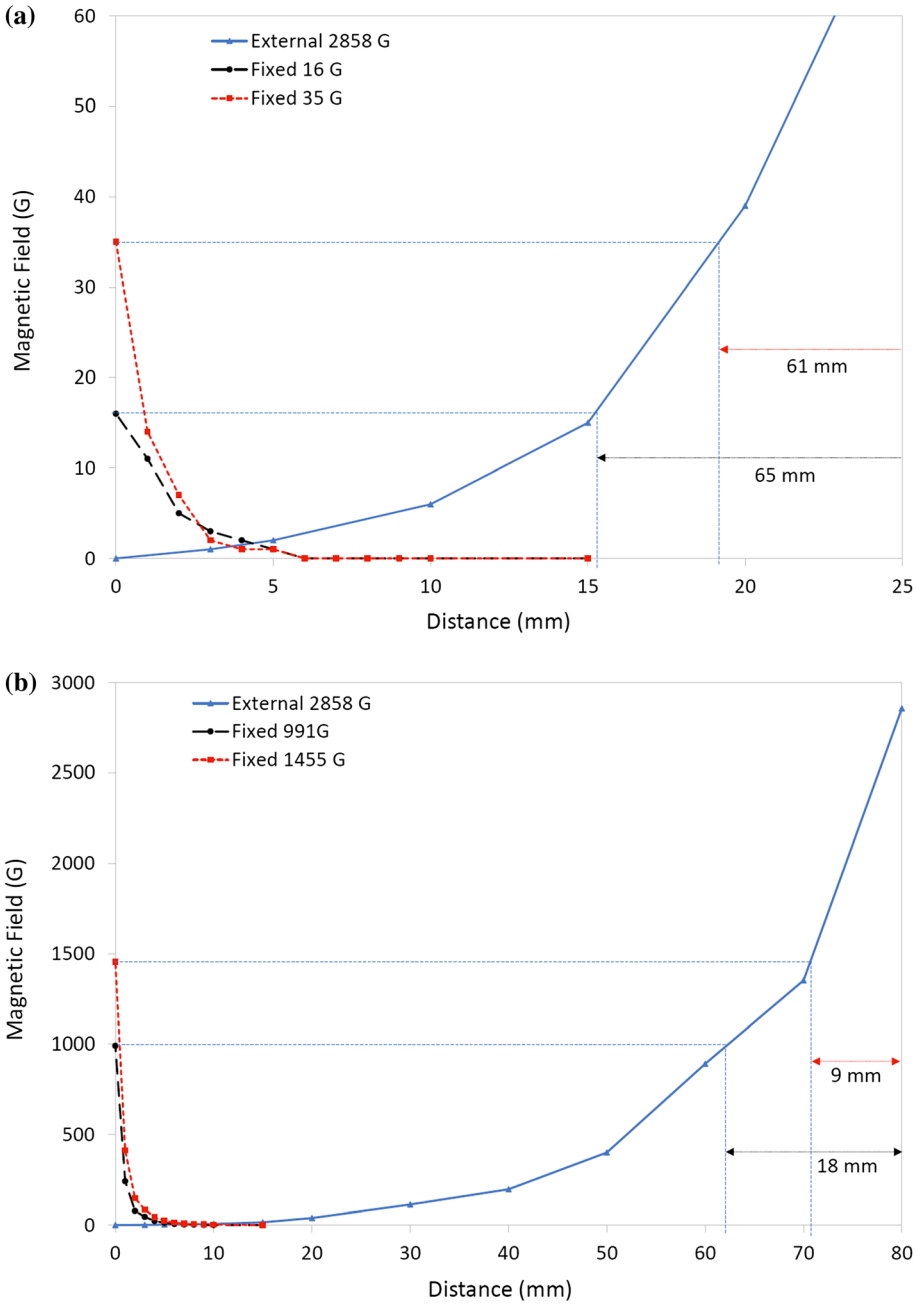

Fig. 8 A comparison between magnetic fields of the 2858 g external magnet and four fixed magnets. The external magnet is initially located at 80 mm away from the fixed magnets

approximately 69 mm from the 35 G fixed magnet its magnetic field becomes stronger than that of the fixed magnet and moves the iron oxide particles to the outer end of the reservoir. To move the attached to the 991 G fixed magnet, the 3839 G external magnet needs to be within a distance of 38 mm. This distance for the 1455 G fixed magnet requires to be about 31 mm.

The characterized distances would be a guideline for a user of the developed magnetometer to determine the strength of a magnetic field. The user would also be able to visually determine the direction of the external magnetic field. With a strong enough magnetic field the device can be used to determine where a magnetic field lies in regards to X, Y, and Z axis. It is to be noted that if the reservoir block is designed to be thinner, the characterization of the external magnetic fields presented to the device could be more accurate.

5 Conclusions

A powerless iron oxide-based magnetometer was developed to detect magnetic fields, their direction and the range of their strength. Different fixed magnet reservoir

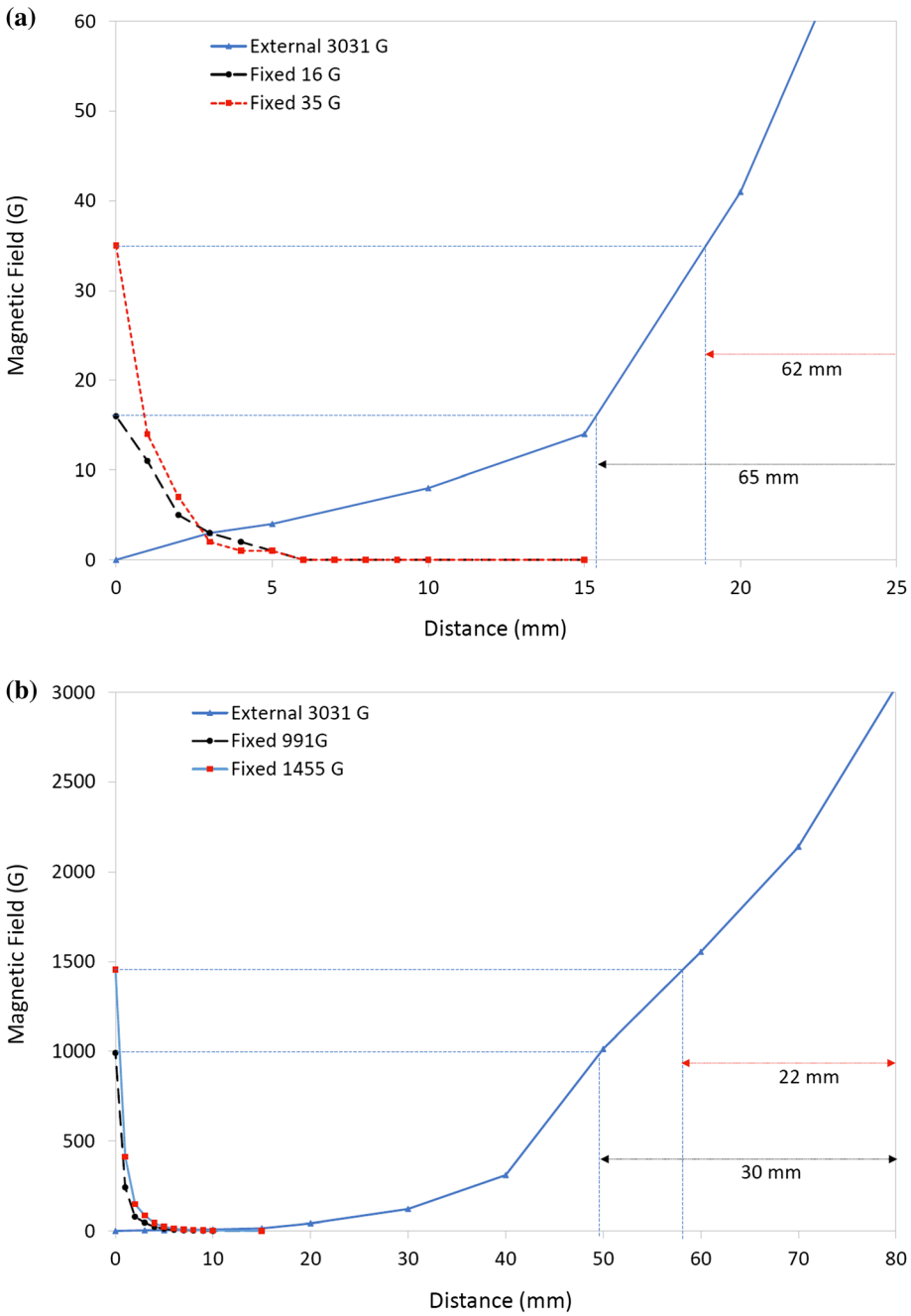

Fig. 9 A comparison between magnetic fields of the 3031 g external magnet and four fixed magnets. The external magnet is initially located at 80 mm away from the fixed magnets

configurations were developed in positive and negative X, Y and Z axes within the range of 16–1455 G. Utilizing the external magnetic field required to displace the iron oxide nanoparticles in each of the four reservoirs on each face of the device allows for a visual determination of the range of the external magnetic field. If the nanoparticles are pulled away only from the 16 G fixed magnet, the rage of the external magnetic field would be between 16 and the 35 G. Similarly, if the nanoparticles are pulled away from both the 16 G and 35 G fixed magnets, the external magnetic field would between 35 G and the strength of the next fixed magnet which is 991 G. This process can be similarly applied for the other configurations, allowing for the visual identification of a magnetic field strength. As the device is simple enough to be fabricated and requires no power to operate, it can be used in several different applications requiring inexpensive solutions for a magnetic field detection, and its strength and direction identification, particularly in remote areas.

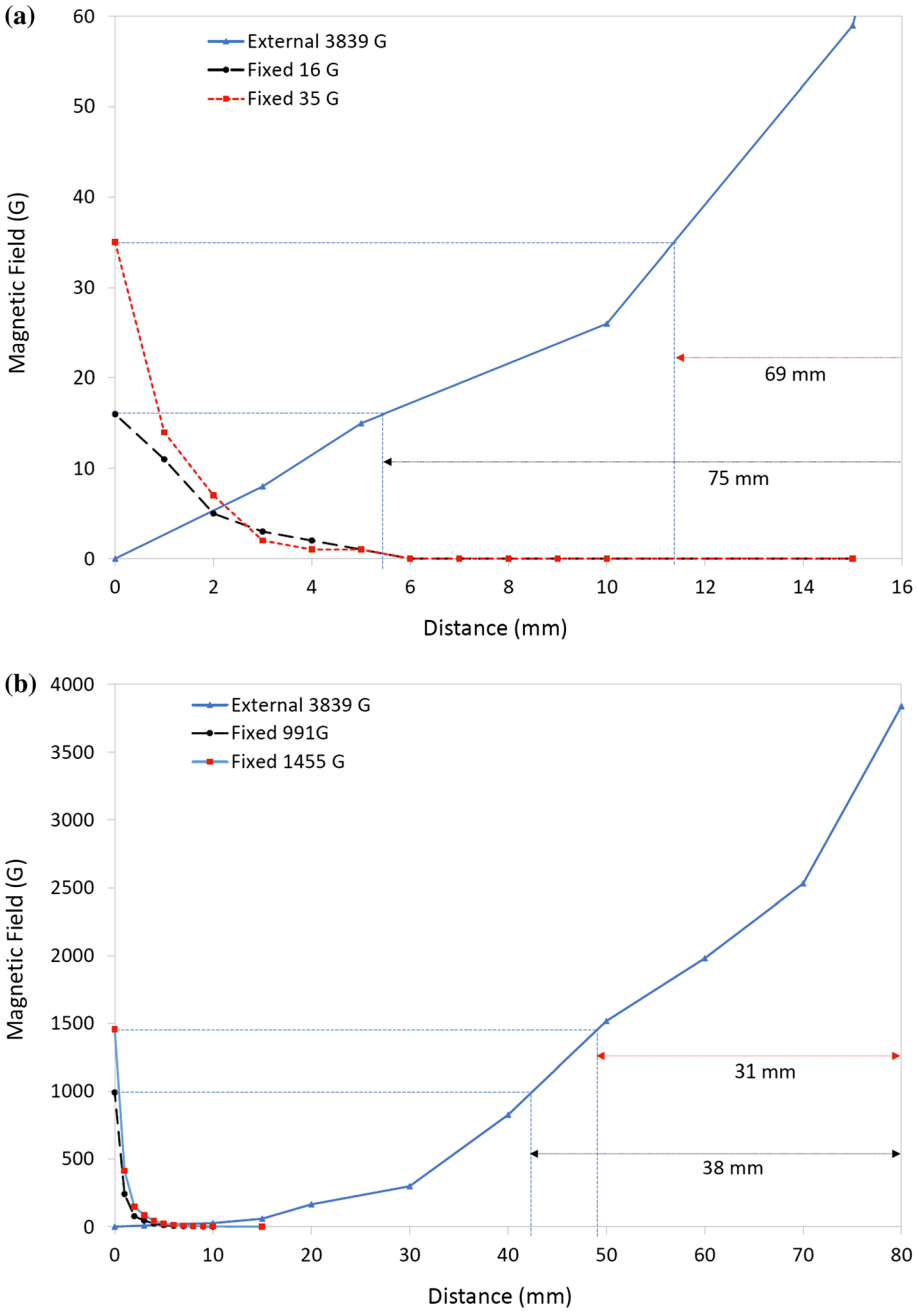

Fig. 10 A comparison between magnetic fields of the 3839 g external magnet and four fixed magnets. The external magnet is initially located at 80 mm away from the fixed magnets

Funding This research was supported by Alfred State Applied Learning Program.

Compliance with ethical standards

Conflict of interest All authors declare that they have no conflict of interest.

References

Auster HU, Glassmeier KH, Magnes W, Aydogar O, Baumjohann W, Constantinescu D, Fischer D, Fornacon KH, Georgescu E, Harvey P, Hillenmaier O (2008) The THEMIS fluxgate magnetometer. Space Sci Rev 141(1–4):235–264

Baltag O (2013) Orthogonal fields controlled fluxgate with ferrofluid. Sensor Lett 11(1):102–105

Biswal RC (2011) Pure and Pt-loaded gamma iron oxide as sensor for detection of sub ppm level of acetone. Sens Actuators B Chem 157(1):183–188

Bower K, Colon R, Karnyski C, Minkel J, Rashidi R (2018) Piezoelectric-based monitoring of restless legs syndrome (RLS). In: International conference on mechatronics and intelligent robotics 2018 May 19. Springer, Cham, pp 923–930

Brown P, Beek T, Carr C, O'Brien H, Cupido E, Oddy T, Horbury TS (2012) Magnetoresistive magnetometer for space science applications. Meas Sci Technol 23(2):025902

Budker D (2003) A new spin on magnetometry. Nature 422(6932):574–575
Budker D, Romalis M (2007) Optical magnetometry. Nat Phys 3(4):227–234
Bulte JW, Kraitchman DL (2004) Iron oxide MR contrast agents for molecular and cellular imaging. NMR Biomed 17(7):484–499
Cabrera L, Gutierrez S, Menendez N, Morales MP, Herrasti P (2008) Magnetite nanoparticles: electrochemical synthesis and characterization. Electrochim Acta 53(8):3436–3441
Cai Y, Zhao Y, Ding X, Fennelly J (2012) Magnetometer basics for mobile phone applications. Electron Prod 54(2):1–3
Cochrane CJ, Blacksberg J, Anders MA, Lenahan PM (2016) Vectorized magnetometer for space applications using electrical readout of atomic scale defects in silicon carbide. Sci Rep 6:37077
Cui N, Wu W, Zhao Y, Bai S, Meng L, Qin Y, Wang ZL (2012) Magnetic force driven nanogenerators as a noncontact energy harvester and sensor. Nano Lett 12(7):3701–3705
Dai J, Yang M, Li X, Liu H, Tong X (2011) Magnetic field sensor based on magnetic fluid clad etched fiber Bragg grating. Opt Fiber Technol 17(3):210–213
Duell T, Muehlbauer M, Seitzinger T, Westfall J, Rashidi R (2018) MEMS capacitive sensor for wound monitoring applications. In: IOP conference series: materials science and engineering 2018 September, vol 417(1). IOP Publishing, New York, p 012040
Fujimaki N, Tamura H, Imamura T, Hasuo S (1988) A single-chip SQUID magnetometer. IEEE Trans Electron Dev 35(12):2412–2418
Gao Y, Huang JP, Liu YM, Gao L, Yu KW, Zhang X (2010) Optical negative refraction in ferrofluids with magnetocontrollability. Phys Rev Lett 104(3):034501
Gao R, Jiang Y, Abdelaziz S (2013) All-fiber magnetic field sensors based on magnetic fluid-filled photonic crystal fibers. Opt Lett 38(9):1539–1541
Hatipoglu G, Tadigadapa S (2015) Micromachined magnetoflexoelastic resonator based magnetometer. Appl Phys Lett 107(19):192406
Hermanek M, Zboril R, Medrik I, Pechousek J, Gregor C (2007) Catalytic efficiency of iron(III) oxides in decomposition of hydrogen peroxide: competition between the surface area and crystallinity of nanoparticles. J Am Chem Soc 129(35):10929–10936
Homa D, Pickrell G (2014) Magnetic sensing with ferrofluid and fiber optic connectors. Sensors 14(3):3891–3896
Ilmoniemi R, Hari R, Reinikainen K (1984) A four-channel SQUID magnetometer for brain research. Electroencephalogr Clin Neurophysiol 58(5):467–473
Ji H, Pu S, Wang X, Yu G (2012) Magnetic field sensing based on V-shaped groove filled with magnetic fluids. Appl Opt 51(8):1010–1020
Jian YC, Zhang LF, Huang JP (2006) Magnetophoresis of ferrofluid in microchannel system and its nonlinear effect. Preprint arXiv: physics/0611135
Kaushik A, Solanki PR, Ansari AA, Sumana G, Ahmad S, Malhotra BD (2009) Iron oxide-chitosan nanobiocomposite for urea sensor. Sens Actuators B Chem 138(2):572–580
Kohout S, Roos J, Keller H (2007) Novel sensor design for torque magnetometry. Rev Sci Instrum 78(1):013903
Kominis IK, Kornack TW, Allred JC, Romalis MV (2003) A subfemtotesla multichannel atomic magnetometer. Nature 422(6932):596–599
Le Contel O, Leroy P, Roux A, Coillot C, Alison D, Bouabdellah A, Mirioni L, Meslier L, Galic A, Vassal MC, Torbert RB (2016) The search-coil magnetometer for MMS. Space Sci Rev 199(1–4):257–282
Lee LP, Char K, Colclough MS, Zaharchuk G (1991) Monolithic 77 K dc SQUID magnetometer. Appl Phys Lett 59(23):3051–3053
Leger JM, Bertrand F, Jager T, Le Prado M, Fratter I, Lalaurie JC (2009) Swarm absolute scalar and vector magnetometer based on helium 4 optical pumping. Proc Chem 1(1):634–637
Li C, Shen Y, Jia M, Sheng S, Adebajo MO, Zhu H (2008) Catalytic combustion of formaldehyde on gold/iron-oxide catalysts. Catal Commun 9(3):355–361
Li Z, Chen S, Zhang S, Guo X, Cao Q (2016) Overhauser magnetometer sensor design for magnetic field observation. In: Radiation detectors: systems and applications XVII 2016 October 3, vol 9969. International Society for Optics and Photonics, New York, p 99690Q
Liu Z, Zhao B, Shi Y, Guo C, Yang H, Li Z (2010) Novel nonenzymatic hydrogen peroxide sensor based on iron oxide–silver hybrid submicrospheres. Talanta 81(4–5):1650–1654
Liu H, Dong H, Liu Z, Ge J, Bai B, Zhang C (2017) Noise characterization for the FID signal from proton precession magnetometer. J Instrum 12(07):P07019
Meyners D, Von Hofe T, Vieth M, Rührig M, Schmitt S, Quandt E (2009) Pressure sensor based on magnetic tunnel junctions. J Appl Phys 105(7):07C914
Pang H, Li J, Chen D, Pan M, Luo S, Zhang Q, Luo F (2013) Calibration of three-axis fluxgate magnetometers with nonlinear least square method. Measurement 46(4):1600–1606
Qiang Y, Antony J, Sharma A, Nutting J, Sikes D, Meyer D (2006) Iron/iron oxide core–shell nanoclusters for biomedical applications. J Nanopart Res 8(3–4):489–496
Rashidi R, Alenezi J, Czechowski J, Niver J, Mohammad S (2019) Graphite-on-paper-based resistive sensing device for aqueous chemical identification. Chem Pap 73(11):2845–2855
Roetenberg D, Slycke P, Ventevogel A, Veltink PH (2007) A portable magnetic position and orientation tracker. Sens Actuators B Phys 135(2):426–432
Russenschuck S (2017) Rotating-and translating-coil magnetometers for extracting pseudo-multipoles in accelerator magnets. COMPEL Int J Comput Math Electr Electron Eng 36:1552–1567
Schwindt PD, Knappe S, Shah V, Hollberg L, Kitching J, Liew LA, Moreland J (2004) Chip-scale atomic magnetometer. Appl Phys Lett 85(26):6409–6411
Tartaj P, Morales MP, Gonzalez-Carreño T, Veintemillas-Verdaguer S, Serna CJ (2011) The iron oxides strike back: from biomedical applications to energy storage devices and photoelectrochemical water splitting. Adv Mater 23(44):5243–5249
Taylor JM, Cappellaro P, Childress L, Jiang L, Budker D, Hemmer PR, Yacoby A, Walsworth R, Lukin MD (2008) High-sensitivity diamond magnetometer with nanoscale resolution. Nat Phys 4(10):810–816
Teja AS, Koh PY (2009) Synthesis, properties, and applications of magnetic iron oxide nanoparticles. Prog Cryst Growth Charact Mater 55(1–2):22–45
Uddin MA, Tsuda H, Wu S, Sasaoka E (2008) Catalytic decomposition of biomass tars with iron oxide catalysts. Fuel 87(4–5):451–459
Wang YX (2011) Superparamagnetic iron oxide based MRI contrast agents: current status of clinical application. Quant Imaging Med Surg 1(1):35
Weinstock H (ed) (2012) SQUID sensors: fundamentals, fabrication and applications. Springer
Xu Q, Seidel M, Paprotny I, White RM, Wright PK (2011) Integrated centralized electric current monitoring system using wirelessly enabled non-intrusive ac current sensors. In: SENSORS, IEEE 2011 October 28. IEEE, New York, pp 1998–2001
Zhou C, Ding L, Wang D, Kuang Y, Jiang D (2011) Thinned fiber Bragg grating magnetic field sensor with magnetic fluid. In:

Photonic microdevices/microstructures for sensing III 2011 May 14, vol 8034. International Society for Optics and Photonics, New York, p 803409

Zu P, Chan CC, Lew WS, Hu L, Jin Y, Liew HF, Chen LH, Wong WC, Dong X (2012) Temperature-insensitive magnetic field sensor based on nanoparticle magnetic fluid and photonic crystal fiber. IEEE Photonics J 4(2):491–498